

**MoO<sub>x</sub>-modified bimetallic alloy nanoparticles for highly efficient  
hydrogen production from hydrous hydrazine**

Qilu Yao, Meng He, Xiaoling Hong, Xiaoliang Zhang, Zhang-Hui Lu\*

*Institute of Advanced Materials (IAM), College of Chemistry and Chemical  
Engineering, Jiangxi Normal University, Nanchang 330022, P.R. China.*

E-mail: luzh@jxnu.edu.cn

**Table S1** Catalysts composition determined by inductively coupled plasma atomic emission spectroscopic (ICP-AES).

<b>Catalysts</b>	<b>Ni/Pt (molar ratio)</b>	<b>Mo (mol%)</b>
Ni <sub>0.2</sub> Pt <sub>0.8</sub> -MoO <sub>x</sub> (16.7mol% Mo)	0.23/0.77	16.3
Ni <sub>0.4</sub> Pt <sub>0.6</sub> -MoO <sub>x</sub> (16.7mol% Mo)	0.38/0.62	16.2
Ni <sub>0.6</sub> Pt <sub>0.4</sub> -MoO <sub>x</sub> (16.7mol% Mo)	0.61/0.39	16.5
Ni <sub>0.8</sub> Pt <sub>0.2</sub> -MoO <sub>x</sub> (16.7mol% Mo)	0.82/0.18	16.8
Ni-MoO <sub>x</sub> (16.7mol% Mo)	~	16.6
Pt-MoO <sub>x</sub> (16.7mol% Mo)	~	16.3

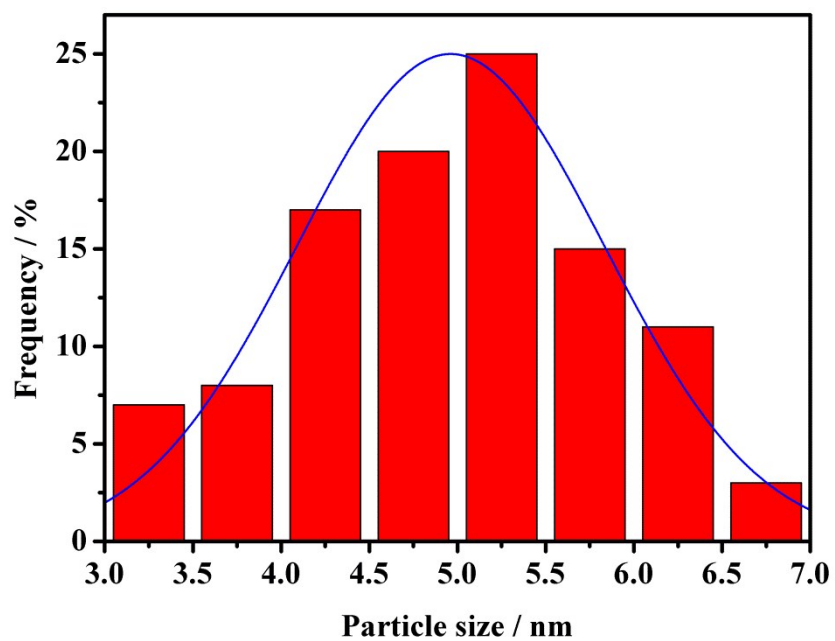


**Fig. S1** Particle size distribution of NiPt-MoO<sub>x</sub> catalyst.

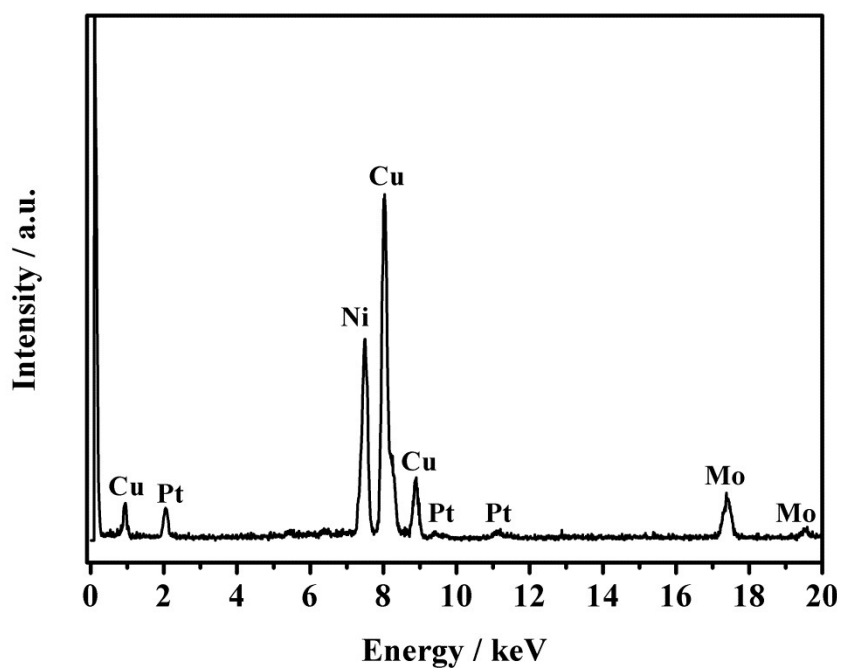


**Fig. S2** The corresponding EDX spectrum of the NiPt-MoO<sub>x</sub> catalyst. The Cu signal originates from Cu grid.

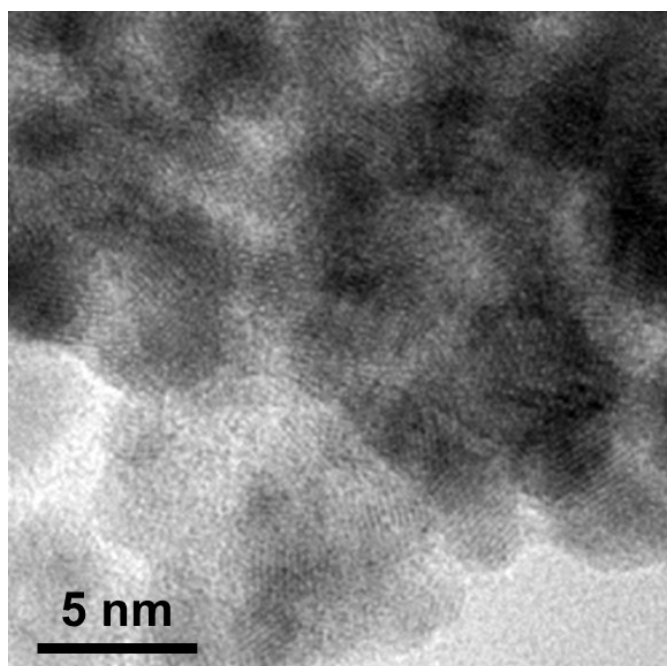


**Fig. S3** HRTEM image of the NiPt-MoO<sub>x</sub> catalyst.

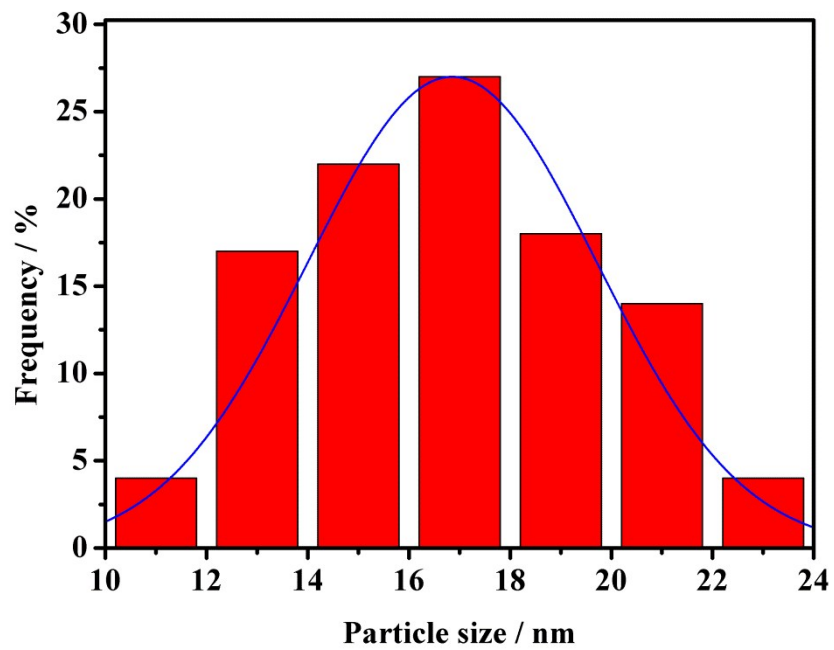


**Fig. S4** Particle size distribution of NiPt catalyst.

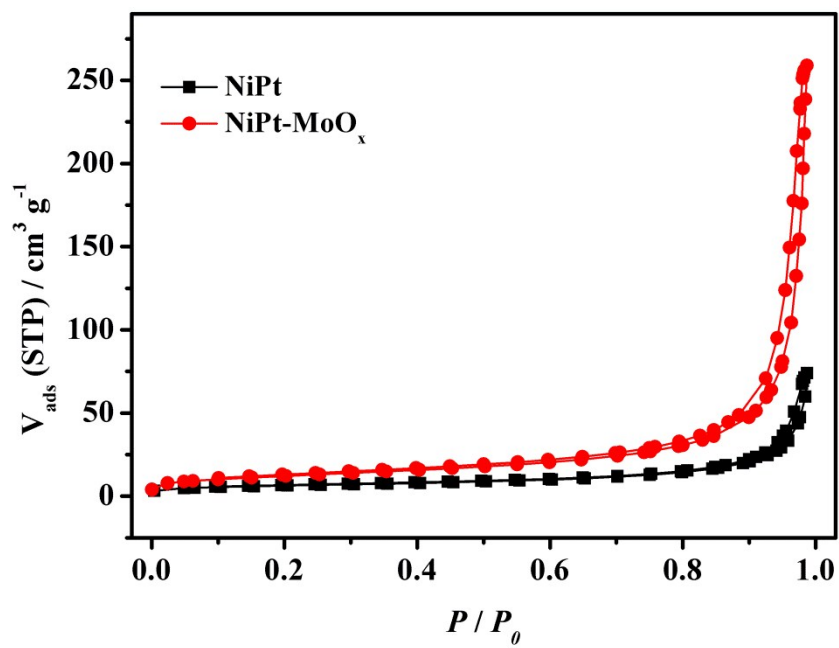


**Fig. S5** N<sub>2</sub> adsorption-desorption isotherms for NiPt-MoO<sub>x</sub> and NiPt catalyst.

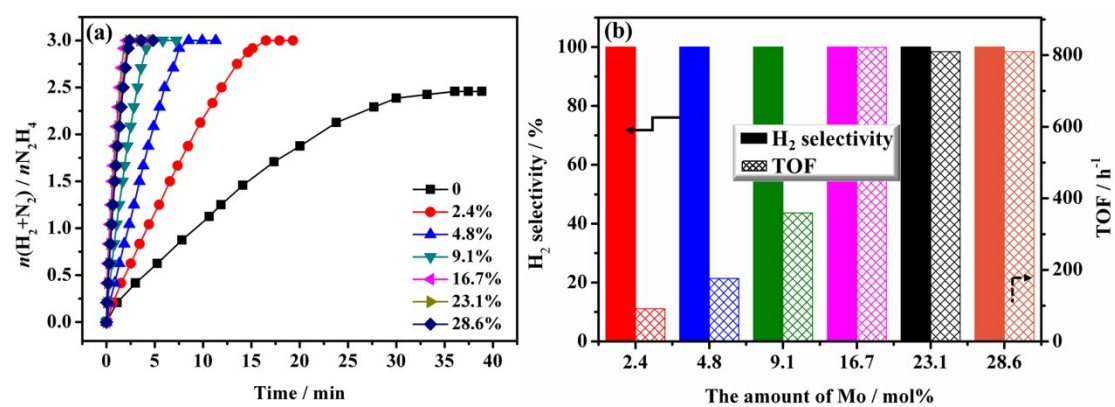


**Fig. S6** (a) Time course plots and (b) the related hydrogen selectivity and TOF values for H<sub>2</sub> evolution from N<sub>2</sub>H<sub>4</sub>·H<sub>2</sub>O (200 mM, 5 mL) decomposition over Ni<sub>0.6</sub>Pt<sub>0.4</sub>-MoO<sub>x</sub> catalysts with different Mo contents in the presence of NaOH (1.0 M) at 323 K.



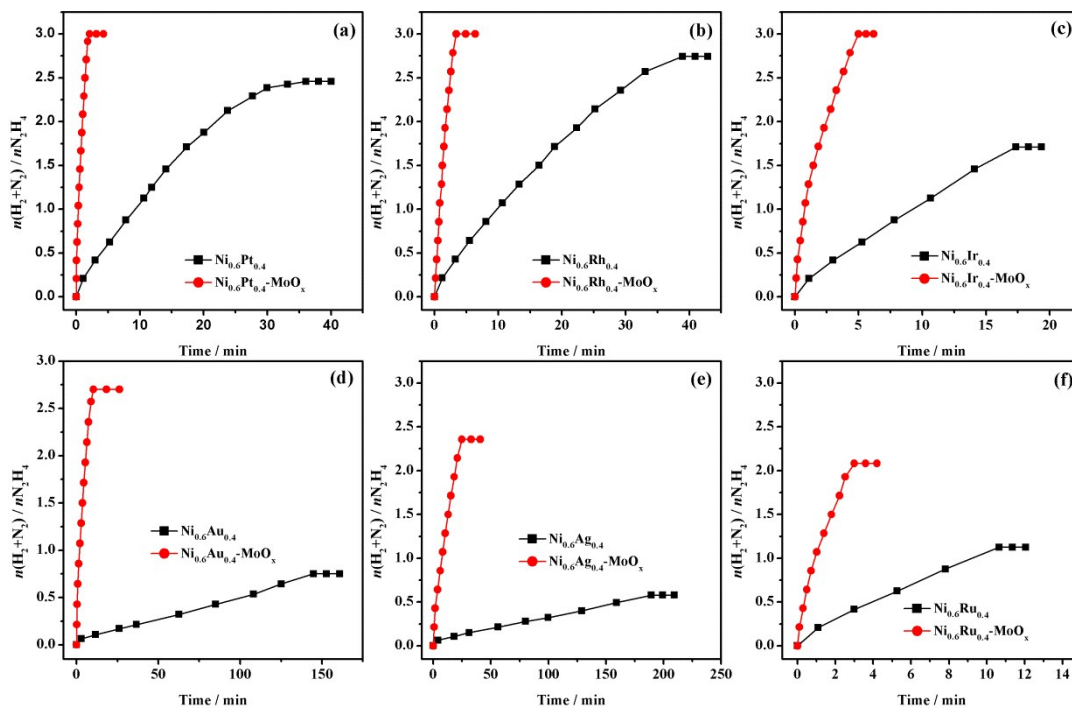


**Fig. S7** Time course plots for H<sub>2</sub> evolution from N<sub>2</sub>H<sub>4</sub>·H<sub>2</sub>O (200 mM, 5 mL) decomposition over Ni<sub>0.6</sub>M<sub>0.4</sub>-MoO<sub>x</sub> and Ni<sub>0.6</sub>M<sub>0.4</sub> (M = Pt, Rh, Ir, Au, Ag, and Ru) catalysts in the presence of NaOH (1.0 M) at 323 K.

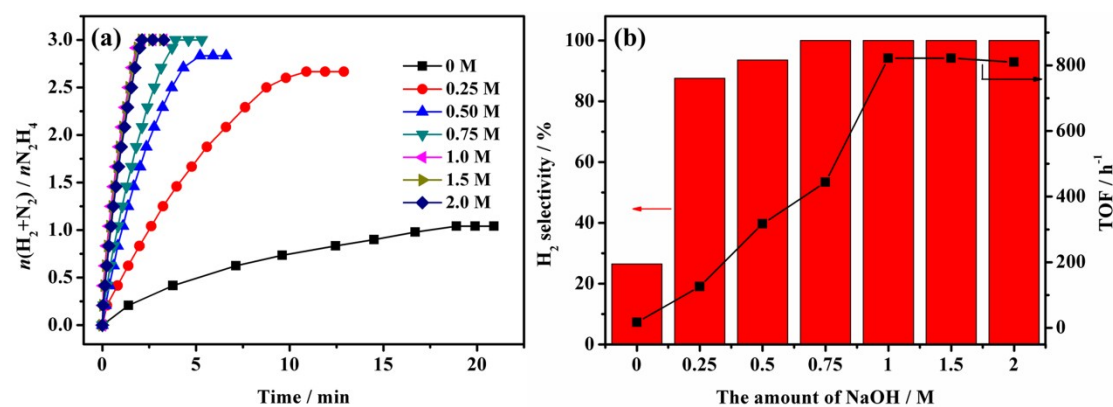


**Fig. S8.** (a) Time course plots and (b) the related hydrogen selectivity and TOF values for  $\text{H}_2$  evolution from  $\text{N}_2\text{H}_4 \cdot \text{H}_2\text{O}$  (200 mM, 5 mL) decomposition over NiPt-MoO<sub>x</sub> catalysts with different concentrations of NaOH at 323 K.

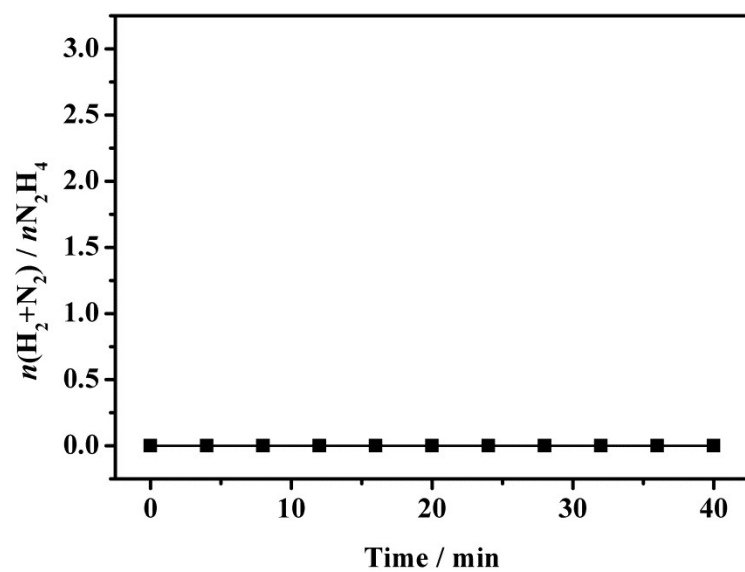


**Fig. S9** Time course plots for H<sub>2</sub> evolution from N<sub>2</sub>H<sub>4</sub>·H<sub>2</sub>O (200 mM, 5 mL) decomposition in the presence of NaOH (1.0 M) at 323 K.

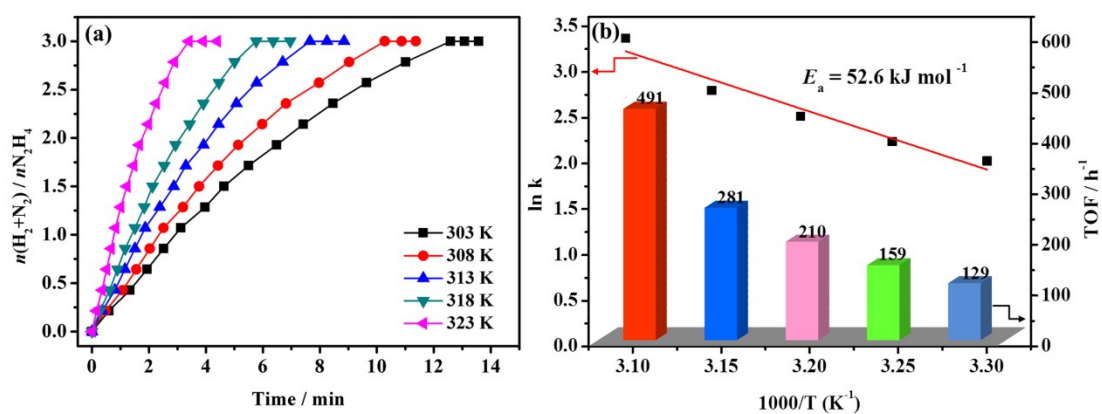


**Fig. S10** (a) Time course plots for H<sub>2</sub> evolution from N<sub>2</sub>H<sub>4</sub> aqueous solution (200 mM, 5 mL) over Ni<sub>0.6</sub>Rh<sub>0.4</sub>-MoO<sub>x</sub> catalyst at different temperatures. (b) The corresponding TOF values and Arrhenius plots ( $\ln k$  versus  $1/T$ ) for H<sub>2</sub> evolution from N<sub>2</sub>H<sub>4</sub> aqueous solution.

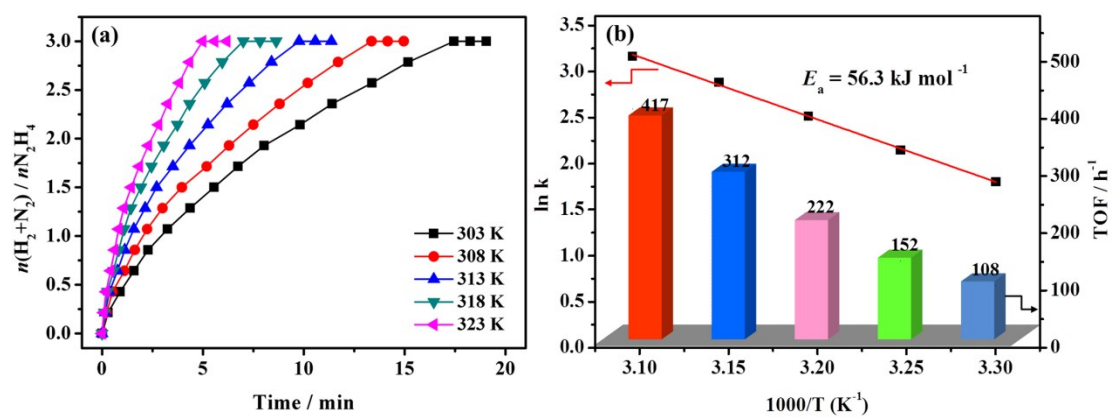


**Fig. S11** (a) Time course plots for H<sub>2</sub> evolution from N<sub>2</sub>H<sub>4</sub> aqueous solution (200 mM, 5 mL) over Ni<sub>0.6</sub>Ir<sub>0.4</sub>-MoO<sub>x</sub> catalyst at different temperatures. (b) The corresponding TOF values and Arrhenius plots ( $\ln k$  versus  $1/T$ ) for H<sub>2</sub> evolution from N<sub>2</sub>H<sub>4</sub> aqueous solution.

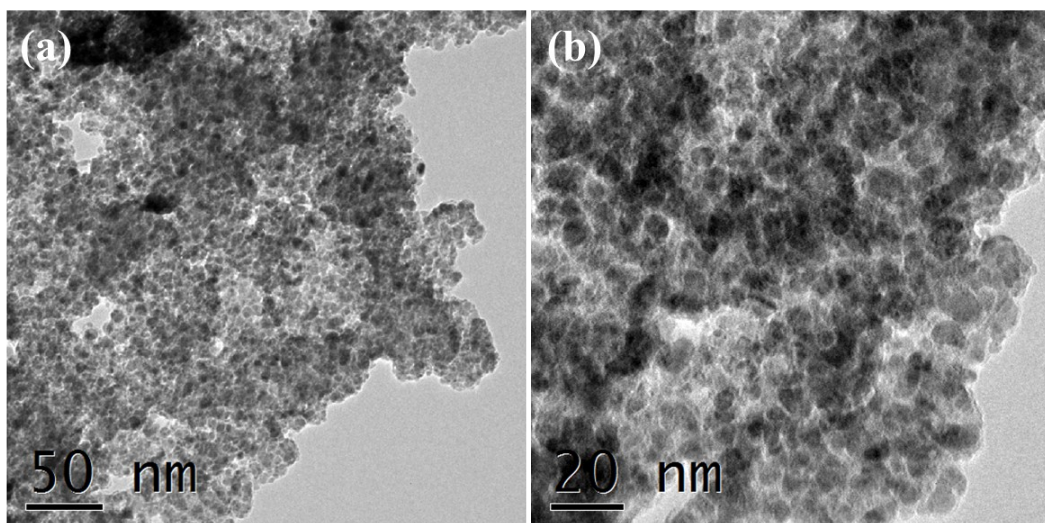


**Fig. S12** TEM images of Ni<sub>0.6</sub>Pt<sub>0.4</sub>-MoO<sub>x</sub> after the durability test.

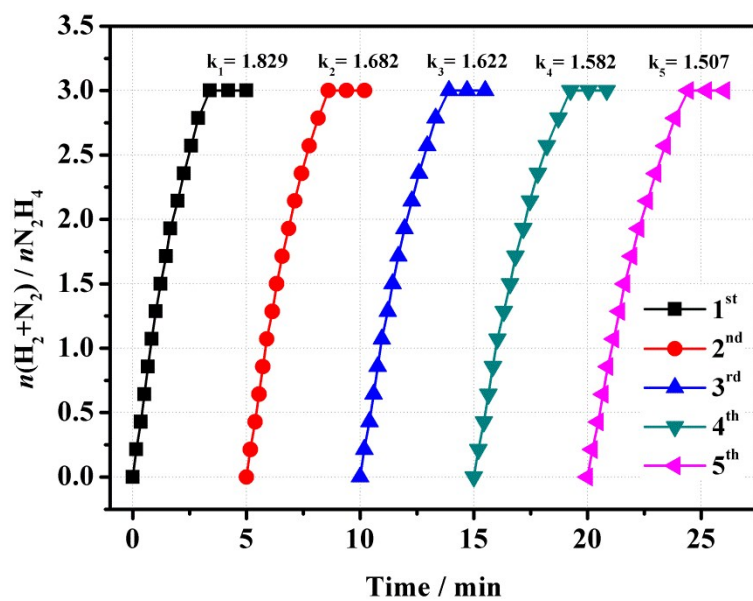


**Fig. S13** Stability test for H<sub>2</sub> evolution from N<sub>2</sub>H<sub>4</sub> aqueous solution (200 mM, 5 mL) over Ni<sub>0.6</sub>Rh<sub>0.4</sub>-MoO<sub>x</sub> NPs at 323 K.

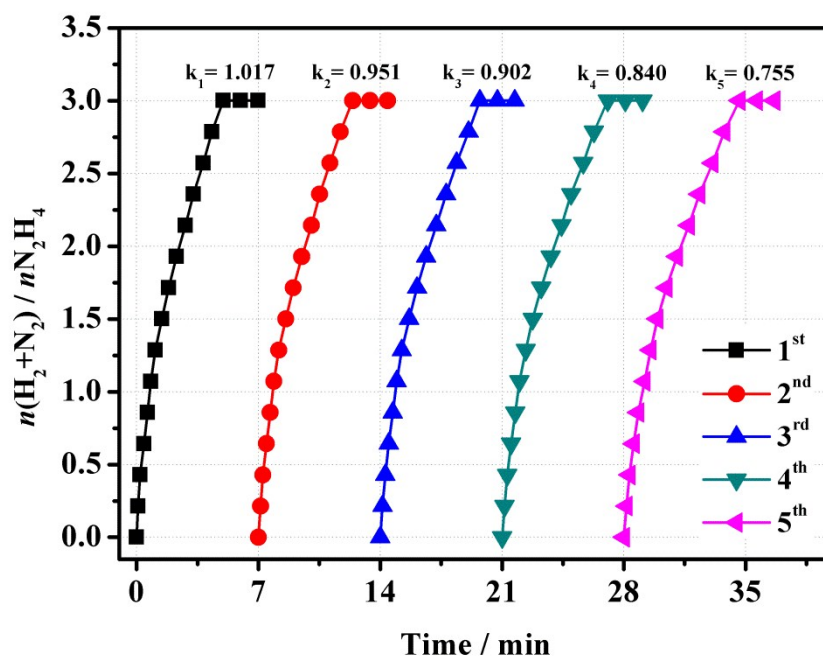


**Fig. S14** Stability test for H<sub>2</sub> evolution from N<sub>2</sub>H<sub>4</sub> aqueous solution (200 mM, 5 mL) over Ni<sub>0.6</sub>Ir<sub>0.4</sub>-MoO<sub>x</sub> NPs at 323 K.



**Table S2** Comparison of activities of different catalysts for hydrogen evolution from  $\text{N}_2\text{H}_4 \cdot \text{H}_2\text{O}$  aqueous solution.

Catalysts	T (K)	$\text{H}_2$ Selectivity (%)	TOF ( $\text{h}^{-1}$ )	$E_a$ ( $\text{kJ mol}^{-1}$ )	Ref.
$\text{Pt}_{0.6}\text{Ni}_{0.4}/\text{PDA-rGO}$	30	100	903	33.39	S1
$\text{Ni}_{0.6}\text{Pt}_{0.4}\text{-MoO}_x$	50	100	822	49.6	This work
$(\text{Ni}_3\text{Pt}_7)_{0.5}\text{-}(\text{MnO}_x)_{0.5}/\text{NPC-900}$	50	100	706	50.15	S2
$\text{Ni}_{0.8}\text{Pt}_{0.2}/\text{MIL-101-NH}_2$	50	100	676	53.2	S3
$\text{Ni}_{40}\text{Pt}_{60}\text{-CNDs}$	50	100	594	43.9	S4
$\text{Ni}_{84}\text{Pt}_{16}/\text{graphene}$	50	100	415	40	S5
$\text{Ni}_3\text{Pt}_7/\text{graphene}$	50	100	416	49.36	S6
$\text{Ni}_{88}\text{Pt}_{12}/\text{MIL-101}$	50	100	350	55.5	S7
$\text{Ni}@/\text{Ni-Pt}/\text{La}_2\text{O}_3$	50	100	312	56.20	S8
$\text{G}_4\text{-OH}(\text{Pt}_{12}\text{Ni}_{48})$	70	100	240	-	S9
$\text{PtNi}/\text{C}$	50	100	210	55.3	S10
$\text{Ni}_3\text{Pt}_7/\text{BNG-1000}$	25	100	199.4	28.4	S11
$\text{Ni}_{87}\text{Pt}_{13}/\text{meso-Al}_2\text{O}_3$	50	100	160	55.7	S12
$\text{Ni}_6\text{Pt}_4\text{-SF}$	25	100	150	-	S13
$\text{Ni}_{80}\text{Pt}_{20}@/\text{ZIF-8}$	50	100	90	-	S14
$\text{Ni}_{0.90}\text{Pt}_{0.05}\text{Rh}_{0.05}/\text{La}_2\text{O}_3$	25	100	45.9	-	S15
$\text{Ni}_{0.9}\text{Pt}_{0.1}/\text{Ce}_2\text{O}_3$	25	100	28.1	42.3	S16
$\text{NiPt}_{0.057}/\text{Al}_2\text{O}_3$	30	99	16.5	34.0	S17

### Calculation method for TOF

The turn over frequency (*TOF*) reported in this work is an apparent *TOF* value based on the number of metal (Ni + Pt) atoms in catalysts, which is calculated from the equation as follows:

$$\text{TOF} = \frac{2P_{\text{atm}}V_{H_2+N_2}/RT}{3n_{\text{Ni+Pt}} \times t} \quad (\text{S1})$$

Where  $P_{\text{atm}}$  is the atmospheric pressure,  $V_{H_2+N_2}$  is the volume of generated gas when the conversion reached 50%,  $R$  is the universal gas constant,  $T$  is the room temperature,  $n_{\text{Ni+Pt}}$  is the total number of moles of (Ni + Pt) atoms in the catalyst and  $t$  is the time in hour when the conversion reached 50%.

## References

- S1 F. Z. Song, Q. L. Zhu and Q. Xu, *J. Mater. Chem. A*, 2015, **3**, 23090–23094.
- S2 B. Xia, T. Liu, W. Luo and G. Cheng, *J. Mater. Chem. A*, 2016, **4**, 5616–5622.
- S3 P. L. Liu, X. J. Gu, Y. Y. Wu, J. Cheng, H. Su, *Int. J. Hydrogen Energy*, 2017, **42**, 19096–19105.
- S4 J. K. Sun and Q. Xu, *ChemCatChem*, 2015, **7**, 526–531.
- S5 Y. Du, J. Su, W. Luo and G. Z. Cheng, *ACS Appl. Mater. Interfaces*, 2015, **7**, 1031–1034.
- S6 N. Cao, L. Yang, C. Du, J. Su, W. Luo and G. Z. Cheng, *J. Mater. Chem. A*, 2014, **2**, 14344–14347.
- S7 N. Cao, J. Su, W. Luo and G. Z. Cheng, *Int. J. Hydrogen Energy*, **2014**, *39*, 9726–9734.
- S8 Y. J. Zhong, H. B. Dai, Y. Y. Jiang, D. M. Chen, M. S. Zhu, X. Li and P. Wang, *J. Power Sources*, 2015, **300**, 294–300.
- S9 K. Aranishi, A. K. Singh and Q. Xu, *ChemCatChem*, 2013, **5**, 2248–2252.
- S10 S. N. Oliaee, C. Zhang, S. Y. Hwang, H. M. Cheung and Z. Peng, *J. Phys. Chem. C*, 2016, **120**, 9764–9772.
- S11 X. Q. Du, C. Du, P. Cai, W. Luo and G. Z. Cheng, *ChemCatChem*, 2016, **8**, 1410–1416.
- S12 Y. Jiang, Q. Kang, J. Zhang, H. B. Dai and P. Wang, *J. Power Sources*, 2015, **273**, 554–560.
- S13 A. K. Singh and Q. Xu, *Int. J. Hydrogen Energy*, 2014, **39**, 9128–9134.
- S14 A. K. Singh and Q. Xu, *ChemCatChem*, 2013, **5**, 3000–3004.
- S15 S. I. O, J. M. Yan, H. L. Wang, Z. L. Wang and Q. Jiang, *J. Power Sources*, **2014**, *262*, 386–390.
- S16 H. L. Wang, J. M. Yan, Z. L. Wang, S. I. O and Q. Jiang, *J. Mater. Chem. A*, 2013, **1**, 14957–14962.
- S17 L. He, Y. Huang, A. Wang, Y. Liu, X. Liu, X. Chen, J. J. Delgado, X. Wang and T. Zhang, *J. Catal.*, **2013**, *298*, 1–9.